Sustainable Energy & Fuels

ROYAL SOCIETY OF CHEMISTRY

PAPER

View Article Online
View Journal | View Issue

Cite this: *Sustainable Energy Fuels*, 2025, **9**, 5227

Destabilization of ammonia borane *via* dual confinement in a cobalt-based Prussian blue analogue

Maëlle Cahu,[ab] Carlos A. Castilla-Martinez,[b] Fabrice Salles,[a] Jérôme Long[ac] and Umit B. Demirci*[b]

Ammonia borane (NH_3BH_3, referred to as AB) contains three protic and three hydridic hydrogen atoms, making it a promising candidate for solid-state hydrogen storage. However, in its pristine form, its practical application is limited by dehydrogenation temperatures exceeding 100 °C and the formation of byproducts with complex compositions. To overcome these limitations, we focused on destabilizing AB through confinement, made possible by using a Prussian blue analogue (PBA) as an oxygen-free host material. We selected the lacunar $Co^{II}[Co^{III}(CN)_6]_{2/3}\square_{1/3}$ (referred to as **CoCo**) PBA due to its high thermal stability and the presence of coordinatively unsaturated Co^{2+} sites (CUS), which offer advantageous features for this purpose. Our results show that **CoCo** effectively confines AB, likely through a dual mechanism, with both chemisorption (where AB would coordinate to Co^{2+} CUS) and physisorption (where AB would be retained within the vacancies of the porous structure). Specifically, we found that approximately two-thirds of the AB would be chemisorbed, while one-third would be physisorbed. These findings highlight the crucial role of Co^{2+} CUS (of an oxygen-free host material) in AB confinement as well as in its isothermal dehydrogenation, likely involving homopolar B–H···H–B interactions.

Received 28th May 2025
Accepted 30th July 2025

DOI: 10.1039/d5se00758e

rsc.li/sustainable-energy

Introduction

There is an urgent need to transition from fossil fuels to cleaner energy resources. Hydrogen H_2 has been a frontrunner for decades as a clean alternative energy carrier, but technological hurdles remain, particularly in ensuring its safe and compact H_2 storage.[1,2] To date, no implementable materials able to store H_2 in practical conditions have emerged.[3]

In this regard, ammonia borane (AB) represents a promising molecular entity for chemical H_2 storage owing to its high content in hydrogen (19.6 wt% H). However, the dehydrogenation of solid-state AB presents two key limitations that hinder its practical use for H_2 storage: (i) moderately high desorption temperatures (100–200 °C) requiring additional energetic input for H_2 release and (ii) a predominant decomposition that releases undesired volatile impurities (*e.g.* ammonia (NH_3) and borazine ($B_3N_3H_6$)) alongside H_2.[4,5] One strategy to address these issues involves confining AB within porous materials to facilitate the dehydrogenation process.[6] In particular, previous studies have focused on confining AB within porous molecule-based materials such as metal–organic frameworks (MOF; see *e.g.* ref. 7–16). While a reduction in the dehydrogenation temperature of confined AB is observed, the underlying mechanisms remain unclear. These effects may arise from enhanced surface tension generated by the MOF microporosity or from a catalytic effect mediated by coordinatively unsaturated sites (CUS) within the framework. Additionally, coordinated solvents on the CUS might play a significant role.[17] Gaining further fundamental understanding of the mechanism involved in AB confinement requires exploration of alternative materials. It is worth mentioning that O-containing linkers in MOFs such as Zn-MOF-74 (ref. 18) and Fe-MIL-53 (ref. 19) destabilize AB by reaction of O of the linker and BH_3 of AB, resulting in B–O bonds.

To address the challenge of limiting the decomposition of confined AB, it is critical to develop porous frameworks that are free of hydrogen and oxygen species, which include cyano-bridged coordination networks. Prussian Blue Analogues (PBA), which are typical representatives of cyano-bridged coordination networks, offer intriguing possibilities that remain largely unexplored for H_2 storage applications.[20] PBA exhibits the general formula $A_aM[M'(CN)_6]_b\square_c\cdot xH_2O$ (where A is an alkali ion, M and M′ are transition metal ions, and □ represents the cyanometallate vacancies that ensure the electroneutrality). In these structures, octahedral $[M'(CN)_6]^{x-}$ complexes are linked through cyano bridges to octahedral M^{n+} ions, creating a 3D cubic porous structure (pore sizes of 4 Å and 7.5 Å). The

[a]*ICGM, Univ Montpellier, CNRS, ENSCM, Montpellier 34293, France*
[b]*Institut Européen des Membranes, IEM – UMR 5635, Univ Montpellier, ENSCM, CNRS, Montpellier, France. E-mail: umit.demirci@umontpellier.fr*
[c]*Institut Universitaire de France (IUF), 1 Rue Descartes, Paris Cedex 05 75231, France*

presence of cyanometallate vacancies indicates that the M^{n+} cation completes its coordination sphere with water molecules, which can be subsequently removed to create CUS, able to interact with various molecular species. Moreover, the nature of the metal ions could be easily modulated without affecting the resulting cubic porous structures, allowing for the accurate determination of the parameters affecting the sorption features. Hence, these porous networks have been investigated for sorbents against water,[21] ammonia,[22] carbon dioxide,[23] sulfur oxide and hydrogen sulfide,[24] methane,[25] propane/xylene[26] and hydrocarbons,[27] as well as H_2.[28,29] For the latter, despite pioneering studies, the enhancement of the H_2 storage features family has been rather limited due to their relatively moderate storage capacity (2–3 wt% H_2) at −196 °C by physisorption measurements. However, upon thermal activation and water removal, PBAs exhibit frameworks free of O and H atoms, an essential feature for stable and efficient AB adsorption and confinement.

To our knowledge, the use of PBA for confining AB and facilitating its controlled H_2 release remains unexplored. In this study, we investigate the potential of PBA as materials for AB confinement and study their role in destabilization within the coordination network. Specifically, we focus on the lacunary $Co^{II}[Co^{III}(CN)_6]_{2/3}\square_{1/3}$ (denoted **CoCo**) as a model system due to its high thermal stability and the presence of Co^{2+} CUS that can react with the nitrogen of AB *via* a coordination bond. Our findings demonstrate that **CoCo** exhibits remarkable capacity for AB confinement, and reveals a dual adsorption mechanism involving both chemisorption (AB coordinated to Co^{2+} CUS) and physisorption (AB confined within the PBA's porosity). Notably, we quantified the proportions of each adsorbed AB species, highlighting the crucial role of Co^{2+} CUS in the confinement process. These insights not only establish a new approach to AB confinement, but also provide a foundation for optimizing hydrogen storage systems by modulating the metal ion nature or employing post-functionalization strategies.

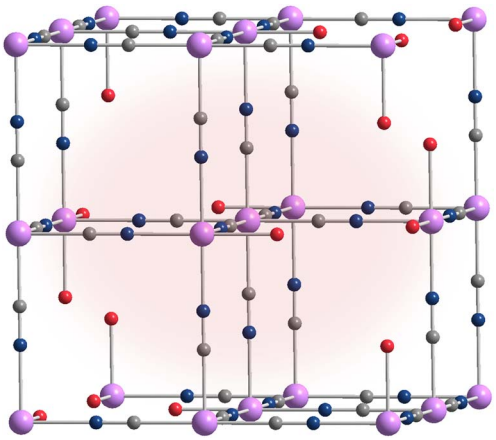

Fig. 1 Crystalline structure of lacunary **CoCo·H_2O**. Color code: lavender, Co; blue, N; grey, C. The oxygen atoms of H_2O coordinated to the Co^{2+} ions are represented by red spheres, whereas interstitial water molecules have been omitted for clarity.

Experimental

Chemical reagents

All chemical reagents were purchased and used without further purification: potassium hexacyanocobaltate(III) $K_3[Co(CN)_6]$ (Aldrich), cobalt(II) nitrate hexahydrate $Co(NO_3)_2\cdot 6H_2O$ (Alfa Aesar, 98%), ammonia borane NH_3BH_3 (Sigma-Aldrich, 97%; denoted as AB), anhydrous dichloromethane CH_2Cl_2 (Sigma-Aldrich, >99.8%), and anhydrous diethyl ether $(C_2H_5)_2O$ (Sigma-Aldrich, >99.7%). Additionally, ultra-pure water with a resistivity of 18.2 MΩ cm was used.

Synthesis of CoCo·H_2O and CoCo

The synthesis of the hydrated lacunar cobalt–cobalt PBA (Fig. 1, denoted as **CoCo·H_2O** hereafter), was carried out by coprecipitation, applying a protocol reported elsewhere.[27] In a flask, a solution of $K_3[Co(CN)_6]$ (30 mmol, 100 mL) was added dropwise for 1 h to a solution of $Co(NO_3)_2\cdot 6H_2O$ (54 mmol, 100 mL) under magnetic stirring at 25 °C. This resulted in the precipitation of **CoCo·H_2O**, which was then washed 12 times with ultra-pure water using centrifugation. Finally, the collected solid was dried at 60 °C for 6 h in an oven. The as-obtained powder exhibits a pink color (Fig. 2). FTIR (ATR): ν(O–H) = 3638 cm^{-1} (coordinated water), ν(O–H) = 3393 cm^{-1} (crystallized water), ν(C≡N) = 2172 cm^{-1} (Co^{III}–C≡N–Co^{II}), ν(O–H) = 1609 cm^{-1} (crystallized water). EDS: 1.45/98.55 (K/Co). Elemental analysis calcd (%) for $Co^{II}[Co^{III}(CN)_6]_{2/3}\square_{1/3}\cdot 4.8H_2O$: C, 16.64; H, 3.35; N, 19.40; found (%): C, 16.38; H, 3.24; N, 18.79.

An activation phase followed,[27] during which **CoCo·H_2O** was transferred to a flask equipped with a cap fitted with a needle. The setup was inserted into a Schlenk line and placed under vacuum while heating at 160 °C for 12 h. During this process, the color of the powder changed. The activated PBA, denoted as **CoCo** hereafter, exhibits a royal blue color (Fig. 2). PBA was then stored in an argon-filled glovebox (O_2 and H_2O: <0.1 ppm) to protect it from exposure to water and prevent its rehydration.

Confinement of AB

Initially, 300 mg of **CoCo** was placed into a Schlenk round-bottom flask within the glovebox. A solution of AB (43 mg) in anhydrous dichloromethane (30 mL) was then added to the flask containing PBA. This ensured a molar ratio of 1 : 1 between **CoCo** and AB. Subsequently, the flask was removed from the glovebox and placed into a cryostat at −20 °C for 2 h under magnetic stirring. Following this, the temperature of the cryostat was increased to 0 °C, and the flask was subjected to dynamic vacuum overnight to evaporate the solvent. Next, the powder was rapidly washed three times on a sintered filter with anhydrous dichloromethane (2 mL for each washing) within the glovebox to remove the excess of AB that was not inserted into the porosity of PBA. The adsorption time of 2 h and the subsequent washing steps of the solid are important to ensure that AB was infiltrated and adsorbed onto the internal surface of PBA. Finally, the resulting powder, denoted as **CoCo·AB**, was

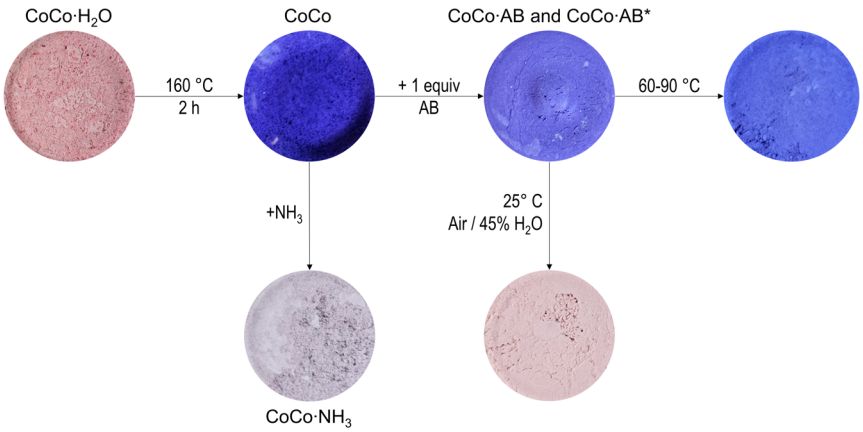

Fig. 2 Color of the different **CoCo**-based materials.

dried under dynamic vacuum overnight and stored at −20 °C. **CoCo·AB** exhibits a dark purple color (Fig. 2).

As mentioned above and as detailed in the next main section, we then aimed at distinguishing the fraction of AB that is chemisorbed onto Co^{2+} CUS and the fraction that is physisorbed (*i.e.* AB confined) within the PBA's porosity. Typically, in a flask and under argon, **CoCo·AB** (33 mg) was dispersed in diethyl ether solvent (6 mL) and the suspension was placed under magnetic stirring. After 24 h, the stirring was stopped, and the supernatant, having extracted the AB molecules weakly attached to the PBA network, was recovered to be analyzed. The as-obtained sample is denoted as **CoCo·AB***. It was finally subjected to a two-day vacuum treatment to remove the solvent.

Characterizations

Fourier-transform infrared (FTIR) spectra on the solid samples were recorded between 4000 cm^{-1} and 650 cm^{-1} using a FTIR Nexus spectrometer from ThermoFisher. A total of 32 spectra were obtained and analyzed using OMNIC software in attenuated total reflection (ATR) mode. Raman measurements (Horiba Jobin Yvon LabRAM 1B; laser Ar/Kr 100 mW 647.1 nm) were also performed. However, the spectra of **CoCo** and **CoCo·AB** (Fig. S1) were similar because of significant fluorescence from the glass vial used due to the air sensitivity of the samples (which hides the B–H and N–H bands in the spectrum, and bands expected to have low intensity).

Liquid-state ^{11}B nuclear magnetic resonance spectroscopy (NMR; $B_0(^1H)$ 400 MHz; $B_0(^{11}B)$ 128.4 MHz) was conducted on AB solutions (see hereafter) using DMSO-d_6 to lock the signal (Sigma-Aldrich, >99%) in a capillary tube. Anhydrous dichloromethane or anhydrous diethyl ether was employed as the solvent, depending on the sample being analyzed. It is worth mentioning that the paramagnetic nature of Co^{II} has not allowed for recording exploitable ^{11}B MAS NMR spectra of the aforementioned solids.

Structural analyses were conducted using powder X-ray diffraction (PXRD). X-ray patterns were acquired with the PANalytical Empyrean M diffractometer in Bragg configuration, covering a range from 10° to 60° in 2θ. The step size was set to 0.026° in 2θ, and each step had a duration of 2700 s. A Co source with a $K_{\alpha 1}$ wavelength of 1.788965 Å was utilized.

The textural properties of **CoCo** were determined by N_2 sorption using a Micromeritics TriFlex apparatus. The specific surface area and the total pore volume were calculated by the Brunauer–Emmett–Teller BET and the Barrett, Joyner and Halenda BJH methods. As both bulk AB and confined AB dehydrogenate upon heating at isothermal conditions, for example at temperatures as low as 70 and 40 °C, respectively, measurements of the textural properties for **CoCo·AB** were not feasible. Indeed, preparing the sample for analysis involves degassing under heating, and this leads to the dehydrogenation of AB.

Energy-dispersive X-ray spectroscopy (EDS) was carried out. The measurements were performed on a scanning electron microscope Quanta 200 Hitachi S-2600N equipped with an Oxford Instruments X-Max 50 mm^2 detector. Element quantification was performed using the INCA software with an acquisition time of 30 s, and all measurements conducted under vacuum conditions. Elemental analyses were conducted using an Elementar Vario MICRO Cube analyzer, with gas chromatography columns developed by Elementar. Additionally, inductively coupled plasma-mass spectroscopy (ICP-MS) analyses were performed using an Agilent 7900 machine. For boron analysis, the machine was operated in "no gas" mode with an analysis time of 0.1 s, and five measurements were taken.

Thermogravimetric and differential thermal analyses (TGA and DTA) were conducted using the thermal analyzer SDT Q600 TA Instruments. The heating process ranged from 25 °C with a heating rate of 5 °C per minute and a N_2 flow of 100 mL min^{-1}. The released gases were analyzed by TG-coupled mass spectrometry (MS; QMS 403 Aëolos Quadro). A hermetically sealed aluminum crucible was used to prevent the samples from exposure to ambient air and moisture, and the crucible lid was pierced just before the analysis to allow the escape of gases.

Isothermal experiments

Isothermal experiments were carried out on **CoCo·AB*** at four different temperatures (60, 70, 80 and 90 °C) using a stainless-

steel reactor equipped with a pressure sensor, enabling continuous monitoring of the pressure evolution inside the reactor. Inside the glovebox, 200 mg of **CoCo·AB*** were placed in a glass vial, which was then put inside the reactor. After sealing, the reactor was transferred outside the glovebox and immersed into a preheated oil bath set to the target temperature, and the pressure was followed. The pressure data were used to calculate the moles of H_2 per mole of AB (equivalents of H_2). For these calculations, the dehydrogenation process was assumed to be isometric, the released gas was considered ideal, and the AB content in **CoCo·AB*** was taken as 8.8 wt% (see Section 3.4). Each experiment was repeated twice to ensure reproducibility.

After the isothermal treatment, the atmosphere inside the reactor was analyzed by gas chromatography (GC) using a PerkinElmer Clarus 400 apparatus equipped with a ShinCarbon ST column. A 100 μL sample was injected into the GC to quantify the H_2 content. This analysis was performed four times to confirm reproducibility. The solid obtained after the isothermal experiment was recovered and analyzed by FTIR spectroscopy.

Results and discussion

CoCo·H_2O

The PBA **CoCo·H_2O**, *i.e.* $Co^{II}[Co^{III}(CN)_6]_{2/3}\square_{1/3}\cdot 4.8H_2O$, with $4.8H_2O$ as determined by both thermogravimetric analysis performed under air (Fig. S2) and elemental analysis, was obtained using the usual self-assembly reactions. The TGA curve shows a single step water loss of up to about 300 °C, indicating that it is not possible to quantitatively discriminate the coordinated and interstitial water molecules. The FTIR spectrum of **CoCo·H_2O** (Fig. 3) displays a characteristic vibration band for the C≡N group at 2172 cm^{-1}, consistent with the formation of a cyano-bridged network.[30] The presence of water molecules is further confirmed by three O–H bands: a stretching band at 3393 cm^{-1} indicative of water crystallized within the PBA network; another stretching band at 3638 cm^{-1} assigned to water molecules coordinated to the Co^{2+}; and a deformation band at 1609 cm^{-1}. The absence of a vibration band at 1385 cm^{-1} confirms the elimination of NO_3^- coming from the reagent $Co(NO_3)_2\cdot 6H_2O$.[31]

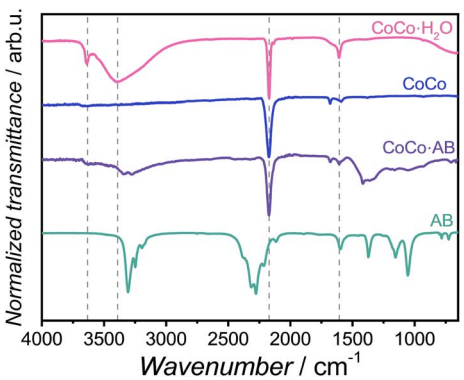

Fig. 3 FTIR spectra of **CoCo·H_2O**, **CoCo** and **CoCo·AB**. For comparative purpose, the spectra for free AB is also given.

The PXRD pattern of **CoCo·H_2O** (Fig. 4) matches with the face-centered cubic (fcc) structure with a space group $Fm\bar{3}m$ (225), consistent with the well-known fcc crystallographic structure of PBA, where the Co^{2+} and Co^{3+} ions are connected through the cyano-bridge forming a 3D cubic structure. Using the Bragg's law and based on the (2 0 0) reflection, the cell parameter a was found to be 10.27 Å.

CoCo

As synthesized, **CoCo·H_2O** incorporates approximately 4.8 water molecules. Some of these water molecules are crystallized within the PBA network, while the remainder are coordinated to the Co^{2+} ions, resulting in an average coordination sphere of $[Co(CN)_4(H_2O)_2]$. However, at the microscopic level, this average formula does not fully capture the distribution of possible environments $[Co(CN)_{6-x}(H_2O)_x]$, with x ranging from 0 to 6, depending on the non-random distribution of vacancies. Solid-state NMR studies of similar PBAs suggest that the actual number of water molecules coordinated to each M^{2+} ion likely varies between 0 and 6, with a typical range of 1–3 water molecules per M^{2+}.[32]

To favor AB adsorption on the Co^{2+} sites of the PBA host material, removal of the water molecules was achieved by heating **CoCo·H_2O** at 160 °C for 12 h under vacuum, yielding the activated lacunar PBA $Co^{II}[Co^{III}(CN)_6]_{2/3}\square_{1/3}$, also denoted as **CoCo**. This process intends to generate Co^{2+} CUS that are highly reactive towards the nitrogen of AB. The activation was visually confirmed by a color change from pink to royal blue (Fig. 2). The blue color likely arises from a minor fraction of Co^{2+} ions adopting a four-coordinated environment. Due to their much higher molar extinction coefficient compared to octahedral Co^{2+}, this minor fraction can dominate the optical response. Moreover, the FTIR spectrum and the TGA curve of **CoCo** showed significant attenuation of the O–H bands (Fig. 3) and the absence of an abrupt weight up to 300 °C (Fig. S2 in comparison to those of **CoCo·H_2O**). The integrity of PBA upon activation was confirmed by the persistence of the C≡N band at 2173 cm^{-1} in the FTIR spectrum (Fig. 3) and the retention of the fcc structure (cell parameter a = 10.09 Å based on the (2 0 0) reflection), as evidenced by the PXRD pattern (Fig. 4). Due to limitations in our experimental setup, it is very challenging to completely isolate the sample from air during transfer from the glovebox to the analysis instruments. This minimal exposure likely explains the presence of weak O–H bands in the FTIR spectrum and the slight deviation (weight loss of about 1 wt% at about 300 °C) observed in the TGA curve.

The textural properties of **CoCo** were determined by N_2 sorption (Fig. S3). According to the IUPAC classification, the adsorption isotherm is of type IV, typical of a mesoporous material. The specific surface area of **CoCo** was found to be as high as 903.6 $m^2\ g^{-1}$. Its total pore volume is 0.80 $cm^3\ g^{-1}$; assuming that the internal volume of **CoCo** can ideally be fully filled by AB (780 mg cm^{-3}). This will require a loading of approximately 620 mg of AB (per gram of **CoCo**).

CoCo·AB

AB was incorporated into CoCo using an impregnation method,[33] which requires a carefully selected solvent. This

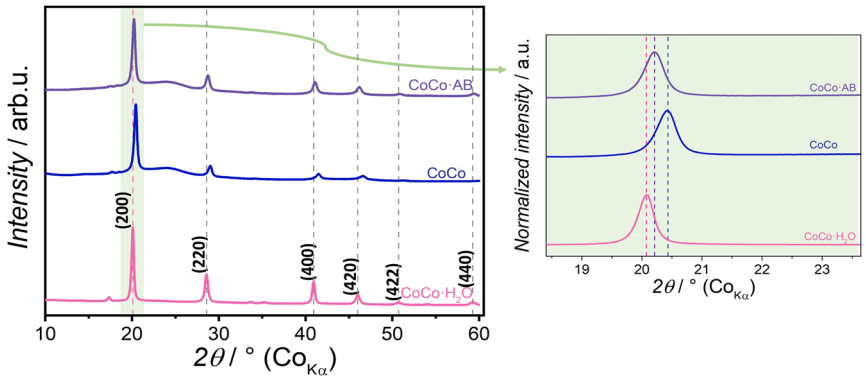

Fig. 4 PXRD for **CoCo·H$_2$O**, **CoCo** and **CoCo·AB**. The right part represents the magnification of the (2 0 0) peak.

solvent needs to meet several criteria simultaneously: it must solubilize the desired loading of AB; it should not compete with AB for reaction on the Co^{2+} CUS of the activated PBA; it should not complex AB (disqualifying tetrahydrofuran[34]); it should lack protic hydrogens to avoid solvolysis of AB (disqualifying *e.g.* methanol[35]); and, a low boiling point is preferred for efficient solvent extraction. Based on these considerations, anhydrous dichloromethane was selected for the confinement of AB by impregnation.

CoCo·AB was obtained through solubilization of AB in anhydrous dichloromethane and reaction with PBA using a 1 : 1 molar ratio. To assess the stability of AB during the impregnation process, the supernatant was sampled and analyzed by ^{11}B NMR. The spectrum (Fig. 4) showed a single signal consisting of a 1 : 3 : 3 : 1 quartet with a chemical shift δ of −22 ppm and a coupling constant $^1J_{B-H}$ of 97 Hz. This is consistent with a BH_3 group and can be viewed as a signature of AB.[36] All of these indicated that AB in dichloromethane is stable during the impregnation of PBA. Otherwise, oligomerization of AB would have resulted in a triplet signal at around −13 ppm due to the presence of BH_2 environments.[37]

The successful impregnation of AB in PBA, forming **CoCo·AB**, was evident from a color shift from royal blue to dark purple (Fig. 2). This observation would suggest a change in the coordination sphere of the Co^{2+} ion. Yet, analysis of the color change is beyond the scope of this work due to the broad nature of the d–d absorption bands involved. Moreover, the change in the coordination sphere might only affect a subset of the Co^{2+} ions.

The FTIR spectrum of **CoCo·AB** (Fig. 3) confirms the structural stability of the PBA network after impregnation with AB, as indicated by the persistence of the C≡N band at 2172 cm^{-1}. Additionally, the spectrum exhibits the main vibration bands characteristic of pure AB, supporting the successful impregnation process. The bands are of weak intensity, which is generally observed for AB confined in the porosity of a host material.[7] Interestingly, a broadening of the N–H deformation bands (1700–1300 cm^{-1}) is observed. This broadening might be attributed to a change in the local environment experienced by the NH_3 group of AB[38] after impregnation within the **CoCo** network.

The PXRD pattern of **CoCo·AB** (Fig. 4) confirmed the integrity of the fcc structure of the host material, indicating that the network remained intact upon AB impregnation. The absence of diffraction peaks related to crystalline AB suggests that AB is located within the porosity of the **CoCo** network as AB in this state does not diffract. This is in line with previous observations on confined AB. Using Bragg's law, the estimated cell parameter a of PBA was determined to be 10.20 Å. This value is slightly lower than that of pristine **CoCo·H$_2$O** (a = 10.27 Å), suggesting that the volume occupied by AB molecules within the porosity is lower than the volume occupied by the water molecules in the as-synthesized **CoCo·H$_2$O**.

The loading of AB in PBA was further confirmed by quantifying the boron content in **CoCo·AB** using ICP-MS. The measured weight percentage of boron was found to be 4.5 wt%, which translates to a weight percentage of 12.85 wt% for AB. This also corresponds to an AB : **CoCo** molar ratio of approximately 0.97 : 1.

CoCo·AB*

Similar to water molecules in **CoCo·H$_2$O**, AB molecules likely occupy two distinct environments. They would be coordinated to Co^{2+} by chemisorption, and/or confined within the porosity of PBA while being physisorbed. To remove the weakly attached AB molecules through diffusion of a solvent, **CoCo·AB** was immersed in anhydrous diethyl ether. This solvent was selected as it could hardly substitute the coordinated AB on the Co^{2+}. The removal of the weakly attached AB molecules by the solvent was evidenced by the presence of the characteristic 1 : 3 : 3 : 1 quartet (δ −22 ppm and $^1J_{B-H}$ of 97 Hz) in the ^{11}B NMR spectrum of the solvent (Fig. S5). The as-obtained sample, denoted as **CoCo·AB***, retained the same color as **CoCo·AB**, although this does not necessarily indicate an identical coordination environment, given the distribution around the Co^{2+} centers. Yet, it appears reasonable that the immersion in anhydrous diethyl ether did not remove the AB molecules coordinated to Co^{2+}. On the other hand, the FTIR spectrum of **CoCo·AB*** (Fig. S6) is comparable to that of **CoCo·AB**, except for the bands in the 1000–1200 cm^{-1} region, which are much more defined for **CoCo·AB***. Since these bands may correspond to Co–NH_3

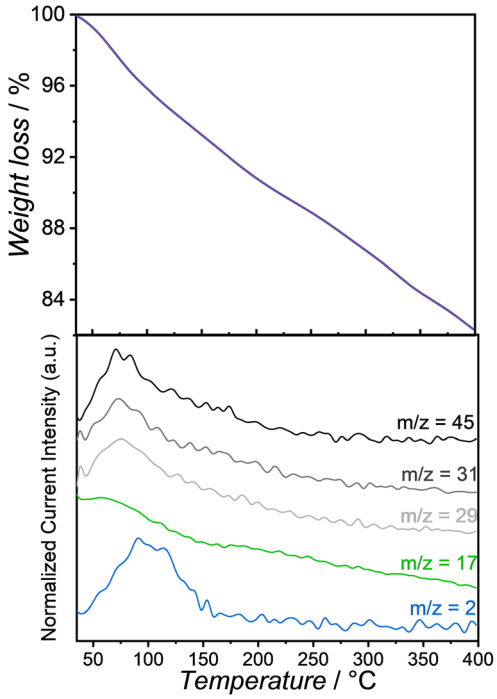

Fig. 5 TGA curve for **CoCo·AB*** under argon, and MS analysis ($m/z = 2$ for H_2, $m/z = 17$ for NH_3 and $m/z = 29$, 31 and 45) for $(C_2H_5)_2O$.

vibrations, this might suggest that the removal of physisorbed AB left only coordinated AB, thereby eliminating the distribution of vibrational modes.

The remaining boron content in **CoCo·AB*** was determined by ICP-MS. It corresponded to 3.1 wt% B, which indicates a weight percentage of AB of 8.8 wt%. In other words, approximately two thirds of the impregnated AB remained within the **CoCo** network, while one-third was removed. This suggests that about two-thirds of the AB molecules would have coordinated to the Co^{2+} CUS, while the remaining one-third would have interacted weakly with the framework. For **CoCo·AB***, the (experimental) molar ratio between the coordinated AB and **CoCo** is approximately 0.63 : 1, suggesting the formula $Co^{II}[Co^{III}(CN)_6]_{2/3}\square_{1/3}\cdot 0.63NH_3BH_3$. This suggests that almost all of the Co^{2+} CUS would be coordinated to one AB molecule.

Dehydrogenation of CoCo·AB*

The thermolytic dehydrogenation of **CoCo·AB*** was investigated by TGA, with the released gases analyzed using MS (Fig. 5). In our experimental conditions, H_2 ($m/z = 2$) started to be released from about 50 °C, and up to about 160 °C. A parallel release of ammonia NH_3 ($m/z = 17$) was also detected, suggesting that a small fraction of AB was dissociated. Additionally, release of diethyl ether ($m/z = 29$, 31 and 45), which was used to wash the **CoCo·AB** sample, was also observed from about 50 °C. These observations lead to two comments. First, despite two days of dynamic vacuum treatment, complete removal of diethyl ether from the sample was not achieved. Second, the total weight loss of 17.7 wt% determined at 400 °C on the TGA analysis is due to H_2, some NH_3 and diethyl ether. It is worth mentioning that the final temperature of 400 °C is excessive, but it was set to ensure that no more H_2 is released above 200 °C. Indeed, AB and destabilized AB are expected to release most of its hydrogen between 50 and 150 °C.[6] Furthermore, **CoCo** is known to slowly decompose above 300 °C,[39] which explains the weight loss that continues above 300 °C. A last observation from the TG curve is that the weight loss is roughly linear, which is typical of AB destabilized by either a catalyst or a surface onto which it is adsorbed,[40,41] knowing that bulk AB and AB not adsorbed onto (or interacting with) a surface shows a stepwise decomposition from about 90 °C.[42,43] This coordination seems to corroborate the coordination of AB with the Co^{2+} CUS discussed above.

Under isothermal conditions (Fig. 6a), **CoCo·AB*** was dehydrogenated in a single step, with the extent of the dehydrogenation increasing as the temperature rose. The amount of gas released at 180 min provides a point of comparison: whereas pristine AB released 0.83 equiv. H_2 at 85 °C, **CoCo·AB*** produced 0.44, 0.67, 0.84 and 1.02 equiv. H_2 at 60, 70, 80 and 90 °C, respectively. The duration of the dehydrogenation process was significantly shorter for **CoCo·AB***, taking approximately 40, 30, 25, and 20 minutes at 60, 70, 80, and 90 °C, respectively. This is a notable improvement compared to pristine AB, which required around 150–200 minutes at 80–90 °C according to references,[44–46] and 180 minutes at 85 °C under our experimental conditions (curve not reported). All of these demonstrate the successful destabilization of AB coordinated to

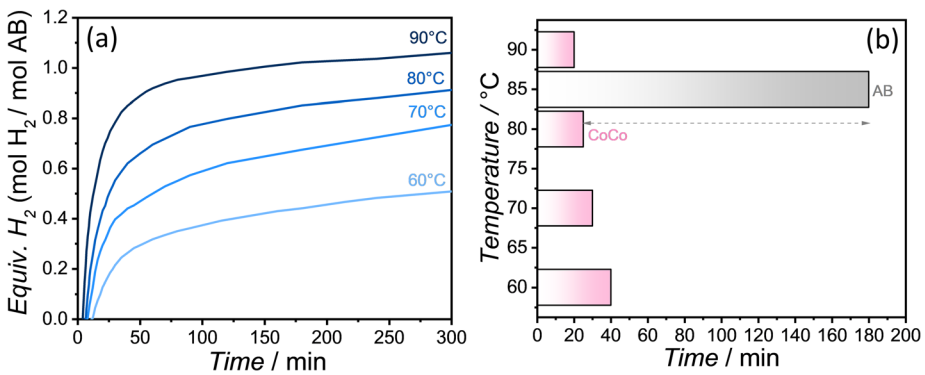

Fig. 6 FTIR spectra of the solids recovered after dehydrogenation of **CoCo·AB*** under isothermal conditions. The bands have been assigned in the colored rectangles.

the Co^{2+} CUS. Indeed, the dehydrogenation process is significantly accelerated, completing in just 20–25 minutes within the same temperature range. This translates to a 6- to 9-fold increase in the dehydrogenation kinetics (Fig. 6b). The dehydrogenation curves (Fig. 6a) were exploited to determine the apparent activation energy using the Arrhenius equation (Fig. S7), yielding a value of 60 kJ mol^{-1}. This value is much lower than the 183 kJ mol^{-1} reported for pristine AB,[47] and is comparable to the 71 kJ mol^{-1} reported for *e.g.* lithium amidoborane $LiNH_2BH_3$, a metal derivative of AB.[48] These findings further confirm the destabilization of confined AB.

The **CoCo·AB*** samples recovered after the isothermal dehydrogenation experiments exhibited a purple color (Fig. 2) and were all analyzed by FTIR spectroscopy (Fig. 7). The presence of residual diethyl ether was confirmed by the C–H stretching bands at around 2800 cm^{-1}. The **CoCo** network remained intact in the dehydrogenation temperature range of 60–90 °C, as indicated by the unchanged C≡N stretching vibrational mode. The B–H stretching mode of AB (2200–2600 cm^{-1}) decreases in intensity as the temperature increases, disappearing at 90 °C. In contrast, the N–H stretching mode (3100–3500 cm^{-1}) also decreased in intensity but remained detectable, even at 90 °C. The disappearance of the B–H stretching mode at 90 °C, alongside the persistence of the N–H stretching mode, suggests that homopolar B–H···H–B dehydrogenation[49] plays a role in the dehydrogenation of **CoCo·AB***.

An additional experiment was conducted by heating **CoCo·AB*** at 150 °C overnight. The recovered solid was analyzed by FTIR spectroscopy (Fig. 8). The dehydrogenated sample still exhibited the N–H stretching vibrational mode, while the B–H stretching mode had disappeared. There were, however, notable changes in the N–H bending mode (1300–1700 cm^{-1}): the band at approximately 1400 cm^{-1} became sharper and more defined, while the bands between 1000 and 1300 cm^{-1} broadened and merged. This last region is associated with the stretching vibrational mode of Co–NH_x.[50]

To further explore this, **CoCo** (*i.e.* free of any guest molecules like both H_2O and AB) was saturated with NH_3 under a stream of N_2 and NH_3, resulting in the sample denoted **CoCo·NH$_3$** (Fig. 2),

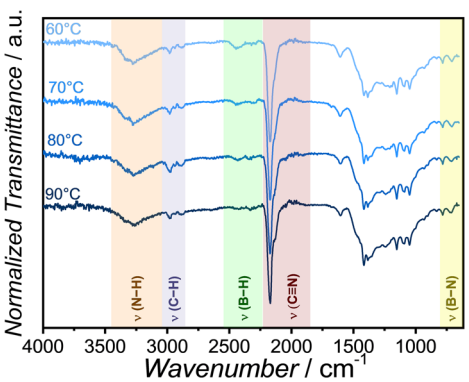

Fig. 7 Dehydrogenation of **CoCo·AB*** under isothermal conditions: (a) evolution of the equivalents of H_2 released at 60, 70, 80 and 90 °C; (b) time dependence of the hydrogen process in AB and **CoCo** as a function of the temperature.

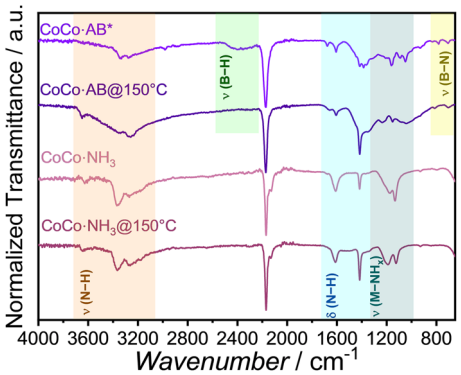

Fig. 8 FTIR spectra of pristine **CoCo·AB***, **CoCo·NH$_3$** and the respective solids recovered after isothermal treatment at 150 °C.

as confirmed by FTIR spectroscopy (Fig. 8). **CoCo·NH$_3$** was then treated at 150 °C under isothermal conditions, and its FTIR spectra were compared with that of **CoCo·AB*** dehydrogenated at the same temperature (Fig. 8). Both spectra exhibited the band associated with Co–NH_x at about 1400 cm^{-1} in the N–H bending region, as well as a small band at around 3650 cm^{-1} in the N–H stretching region (observable in neither **CoCo·NH$_3$** nor **CoCo·AB*** before heating). It is reasonable to conclude that under heating, the likely interaction of NH_x from AB with the Co^{2+} CUS would be more stable than the BH_y moiety, with the latter undergoing more dehydrogenation than the former. A last observation from the FTIR spectrum of **CoCo·AB*** dehydrogenated at 150 °C is that the B–N stretching mode is present, suggesting the formation of the $[NH_xBH_y]_n$ species with $x > y$ and $n \geq 1$.

Stability of CoCo·AB*

The stability of **CoCo·AB*** at room temperature and under an argon atmosphere (in the glove box; Fig. S8) was monitored over time (after 1 day and 6 days). No significant changes were observed by FTIR spectroscopy, indicating that **CoCo·AB*** is stable under these conditions.

When exposed for a duration of 4 hours to flowing air (200 mL min^{-1}) with controlled humidity (42%) and at 25 °C, **CoCo·AB*** evolved. Its color changed from deep purple to dark pink, distinct from the bright pink color of **CoCo·H$_2$O** (Fig. 2). The FTIR spectrum (Fig. 9) resembled a combination of the spectra of 'fresh' **CoCo·AB*** and **CoCo·H$_2$O**. This suggests that partial substitution of AB coordinated to the Co^{2+} CUS by H_2O occurred. **CoCo·AB*** is thus not stable in the presence of moisture, indicating that H_2O is a stronger Lewis base than AB. The N–B bond in AB seems to weaken the Lewis basicity of NH_3 in AB, which contrasts with the well-known stronger basicity of free NH_3 compared to H_2O in coordination chemistry. Furthermore, the presence of B–O bonds in the 1000–1200 cm^{-1} region of the spectrum cannot be ruled out, likely due to the rapid hydration and/or hydrolysis of the BH_3 moiety of the AB molecule.[51] The persistence of N–H vibrational modes suggests that the substitution by water was not complete within the 4 hours exposure period.

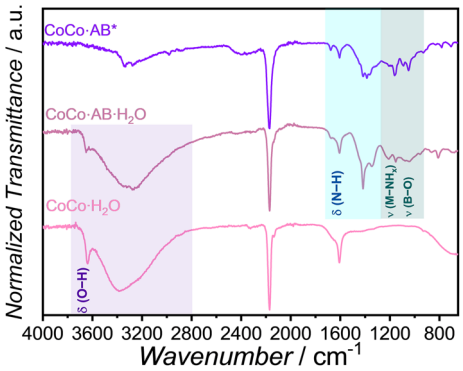

Fig. 9 FTIR spectra of CoCo·AB* after contact with a flow of humidified air, denoted as CoCo·AB*·H_2O. The spectra of CoCo·H_2O and CoCo·AB* are also shown for clarity. The bands have been assigned by the colored rectangles.

Conclusions

Although it is known as a first coordination network, PBA stands out as a material for the confinement of AB towards hydrogen storage applications. Employing a model lacunar PBA, $Co^{II}[Co^{III}(CN)_6]_{2/3}\square_{1/3}$, we hypothesized a dual adsorption mechanism for AB confinement involving both chemisorption (*i.e.* AB coordinated to Co^{2+} CUS) and physisorption (*i.e.* AB confined within the PBA porosity). Our conclusion is notably based on the following observations. We quantified the proportions of the chemisorbed and physisorbed AB species, found to be about 2/3 and 1/3 of the confined AB, respectively, which reasonably underscore the crucial role of Co^{2+} CUS in this process. To our knowledge, this is the first time that such mechanism is proposed and discussed for the confinement of AB, and future works are expected to focus on detailed characterization of the adsorption mechanism from the view point of coordination chemistry.

We also provide further insights into the hydrogen release mechanism, with the likely occurrence of homopolar B–H···H–B dehydrogenation leading to the $[NH_xBH_y]_n$ species with $x > y$ and $n \geq 1$. This offers promising perspectives to modulate the nature of the transition metal ions or using a post-functionalization rationale to optimize the AB confinement and control its dehydrogenation.

Conflicts of interest

There are no conflicts to declare.

Data availability

The authors confirm that the data supporting the findings of this study are available within the article and its supplementary materials. Raw data were generated at The University of Montpellier, CNRS, and ENSCM. Derived data supporting the findings of this study are available from the corresponding author, Umit B. DEMIRCI, on request. The data that support the findings of this study will be openly available in **https://hal.umontpellier.fr/**, upon acceptance for publication and attribution of a DOI.

Fig. S1–S8. See DOI: **https://doi.org/10.1039/d5se00758e**.

Acknowledgements

This work benefited from the aid of La Région Occitanie and Défi Clé Hydrogène Vert (CONDOR project). C.A. Castilla-Martinez and U.B. Demirci acknowledge the France state managed by the Agence Nationale pour la Recherche (ANR) under France 2030 (ref. ANR-22-PEHY-0007). J. Long also acknowledges the support from the Institut Universitaire de France. The authors acknowledge the contribution of Mrs Aurore Larquey, who participated in this project during her internship under the supervision of Dr Maëlle Cahu and Dr Fabrice Salles; her assistance in performing a few syntheses for Dr Maëlle Cahu was appreciated.

Notes and references

1 S. Bosu and N. Rajamohan, *Int. J. Hydrogen Energy*, 2024, **52**, 352–370.
2 L. Mulky, S. Srivastava, T. Lakshmi, E. R. Sandadi, S. Gour, N. A. Thomas, S. S. Priya and K. Sudhakar, *Mater. Chem. Phys.*, 2024, **325**, 129710.
3 M. Yang, S. Berrettoni, B. Sprecher and B. Wang, *Clean Energy*, 2023, **7**, 190–216.
4 J. Huo, K. Zhang, H. Wei, L. Fu, C. Zhao, C. He and X. Hu, *Chin. Chem. Lett.*, 2023, **34**, 108280.
5 R. Kumar, A. Karkamkar, M. Bowden and T. Autrey, *Chem. Soc. Rev.*, 2019, **48**, 5350–5380.
6 K. Turani-I-Belloto, C. A. Castilla-Martinez, D. Cot, E. Petit, S. Benarib and U. B. Demirci, *Int. J. Hydrogen Energy*, 2021, **46**, 7351–7370.
7 Z. Li, G. Zhu, G. Lu, S. Qiu and X. Yao, *J. Am. Chem. Soc.*, 2010, **132**, 1490–1491.
8 S. Gadipelli, J. Ford, W. Zhou, H. Wu, T. J. Udovic and T. Yildirim, *Chem.–Eur. J.*, 2011, **17**, 6043–6047.
9 X. L. Si, L. X. Sun, F. Xu, C. L. Jiao, F. Li, S. S. Liu, J. Zhang, L. F. Song, C. H. Jiang, S. Wang, Y. L. Liu and Y. Sawada, *Int. J. Hydrogen Energy*, 2011, **36**, 6698–6704.
10 R. Q. Zhong, R. Q. Zou, T. Nakagawa, M. Janicke, T. A. Semelsberger, A. K. Burrell and R. E. del Sesto, *Inorg. Chem.*, 2012, **51**, 2728–2730.
11 L. Gao, C. Y. V. Li, H. Yung and K. Y. Chan, *Chem. Commun.*, 2013, **49**, 10629–10631.
12 H. M. Jeong, W. H. Shin, J. H. Park, J. H. Choi and J. K. Kang, *Nanoscale*, 2014, **6**, 6526–6530.
13 X. Wang, L. Xie, K. W. Huang and Z. Lai, *Chem. Commun.*, 2015, **51**, 7610–7613.
14 J. Y. Chung, C. W. Liao, Y. W. Chang, B. K. Chang, H. Wang, J. Li and C. Y. Wang, *J. Phys. Chem. C*, 2017, **121**, 27369–27378.
15 S. Peil, D. Wisser, M. Stähle, P. K. Rossmann, Y. S. Avadhut and M. Hartmann, *J. Phys. Chem. C*, 2021, **125**, 9990–10000.

16 G. L. Li, A. K. Tripathi, H. Chan, S. T. Chen, J. T. Chang, T. Nakagawa and C. Y. Wang, *ACS Sustain. Chem. Eng.*, 2023, **11**, 6143–6152.
17 Y. J. Wu and C. Y. Wang, *ACS Sustain. Chem. Eng.*, 2019, **7**, 16013–16025.
18 S. Gadipelli, J. Ford, W. Zhou and T. Yildirim, *Int. J. Hydrogen Energy*, 2012, **37**, 3633–3638.
19 G. Srinivas, W. Travis, J. Ford, H. Wu, Z. X. Guo and T. Yildirim, *J. Mater. Chem. A*, 2013, **1**, 4167–4172.
20 W. J. Li, C. Han, G. Cheng, S. L. Chou, H. K. Liu and S. X. Dou, *Small*, 2019, **15**, 1900470.
21 L. Boudjema, J. Long, F. Salles, J. Larionova, Y. Guari and P. Trens, *Chem.–Eur. J.*, 2019, **25**, 479–484.
22 A. Takahashi, H. Tanaka, D. Parajuli, T. Nakamura, K. Minami, Y. Sugiyama, Y. Hakuta, S. I. Ohkoshi and T. Kawamoto, *J. Am. Chem. Soc.*, 2016, **138**, 6376–6379.
23 J. T. Culp, C. Madden, K. Kauffman, F. Shi and C. Matranga, *Inorg. Chem.*, 2013, **52**, 4205–4213.
24 P. K. Thallapally, R. K. Motkuri, C. A. Fernandez, B. P. McGrail and G. S. Behrooz, *Inorg. Chem.*, 2010, **49**, 4909–4915.
25 B. Zamora, J. Roque, J. Balmaseda and E. Reguera, *Z. Anorg. Allg. Chem.*, 2010, **636**, 2574–2578.
26 G. Autie-Castro, M. Autie, E. Reguera, R. Moreno-Tost, E. Rodríguez-Castellón, A. Jiménez-López and J. Santamaría-González, *Appl. Surf. Sci.*, 2011, **257**, 2461–2466.
27 L. Boudjema, E. Mamontova, J. Long, J. Larionova, Y. Guari and P. Trens, *Inorg. Chem.*, 2017, **56**, 7598–7601.
28 S. S. Kaye and J. R. Long, *J. Am. Chem. Soc.*, 2005, **127**, 6506–6507.
29 J. T. Culp, S. Natesakhawat, M. R. Smith, E. Bittner, C. Matranga and B. Bockrath, *J. Phys. Chem. C*, 2008, **112**, 7079–7085.
30 A. Ludi and H. U. Güdel, *Helv. Chim. Acta*, 1968, **51**, 2006–2016.
31 M. H. Brooker and D. E. Irish, *Can. J. Chem.*, 1971, **49**, 1289–1295.
32 M. B. Zakaria and T. Chikyow, *Coord. Chem. Rev.*, 2017, **352**, 328–345.
33 A. Gutowska, L. Li, Y. Shin, C. M. Wang, X. S. Li, J. C. Linehan, R. S. Smith, B. D. Kay, B. Schmid, W. Shaw, M. Gutowski and T. Autrey, *Angew. Chem., Int. Ed.*, 2005, **44**, 3578–3582.
34 D. J. Ingram, T. F. Headen, N. T. Skipper, S. K. Callear, M. Billing and A. Sella, *Phys. Chem. Chem. Phys.*, 2018, **20**, 12200–12209.
35 P. V. Ramachandran and P. D. Gagare, *Inorg. Chem.*, 2007, **46**, 7810–7817.
36 J. Hannauer, U. B. Demirci, C. Geantet, J. M. Herrmann and P. Miele, *Phys. Chem. Chem. Phys.*, 2011, **13**, 3809–3818.
37 W. J. Shaw, J. C. Linehan, N. K. Szymczak, D. J. Heldebrant, C. Y. Yonker, D. M. Camaioni, T. Baker and T. Autrey, *Angew. Chem., Int. Ed.*, 2008, **47**, 7493–7496.
38 A. Paolone, F. Teocoli, S. Sanna, O. Palumbo and T. Autrey, *J. Phys. Chem. C*, 2013, **117**, 729–734.
39 P. J. Zambiazi, G. de O. Aparecido, T. de B. Ferraz, W. J. S. Skinner, R. G. Yoshimura and D. E. B. Moreira, *Dalton Trans.*, 2020, **49**, 16488–16497.
40 F. Toche, R. Chiriac, U. B. Demirci and P. Miele, *Int. J. Hydrogen Energy*, 2012, **37**, 6749–6755.
41 G. Moussa, U. B. Demirci, S. Malo, S. Bernard and P. Miele, *J. Mater. Chem. A*, 2014, **2**, 7717–7722.
42 B. Roy, J. Manna and P. Sharma, *J. Alloys Compd.*, 2015, **645**, S234–S238.
43 C. Astorino, E. De Nardo, S. Lettieri, G. Ferraro, M. Bartoli, M. Etzi, A. M. Chiodoni, C. F. Pirri and S. Boccchini, *Polymers*, 2024, **16**, 3471.
44 D. J. Heldebrant, A. Karkamkar, N. J. Hess, M. Bowden, S. Rassat, F. Zheng, K. Rappe and T. Autrey, *Chem. Mater.*, 2008, **20**, 5332–5336.
45 M. Bowden, T. Autrey, I. Brown and M. Ryan, *Curr. Appl. Phys.*, 2008, **8**, 498–500.
46 A. C. Gangal, P. Kale, R. Edla, J. Manna and P. Sharma, *Int. J. Hydrogen Energy*, 2012, **37**, 6741–6748.
47 X. Kang, Z. Fang, L. Kong, H. Cheng, X. Yao, G. Lu and P. Wang, *Adv. Mater.*, 2008, **20**, 2756–2759.
48 J. Chen, T. He, G. Wu, Z. Xiong and P. Chen, *Int. J. Hydrogen Energy*, 2013, **38**, 10944–10949.
49 D. J. Wolstenholme, J. T. Titah, F. N. Che, K. T. Traboulsee, J. Flogeras and G. S. McGrady, *J. Am. Chem. Soc.*, 2011, **133**, 16598–16604.
50 D. G. Hill and A. F. Rosenberg, *J. Chem. Phys.*, 1956, **24**, 1219–1231.
51 G. Moussa, R. Moury, U. B. Demirci and P. Miele, *Int. J. Hydrogen Energy*, 2013, **38**, 7888–7895.